AN ELECTROCHEMICAL ANALYSIS OF SOLID ELECTROLYTE/ELECTRODE SYSTEMS

J.D. Canaday, A.K. Kuriakose, A. Ahmad, and T.A. Wheat

Mineral Processing Laboratory

MINERAL SCIENCES LABORATORIES
CANMET REPORT 86-8E

August 1986

Available in Canada through

Associated Bookstores
and other booksellers

or by mail from

Canadian Government Publishing Centre
Supply and Services Canada
Ottawa, Canada K1A 0S9

Catalogue No. M38-13/86-8E Canada: $3.95
ISBN 0-660-12510-2 Other Countries: $4.75

Price subject to change without notice

AN ELECTROCHEMICAL ANALYSIS OF SOLID ELECTROLYTE/ELECTRODE SYSTEMS

J.D. Canaday*, A.K. Kuriakose*, A. Ahmad*, and T.A. Wheat*

Abstract

The three-phase cell consisting of reactant gases, porous electrodes, and a solid electrolyte is described in electrochemical terms. Electrode processes that cause polarization phenomena are also discussed. The use of two-probe and three-probe techniques is presented together with examples of results obtained for a number of systems.

*Research Scientists, Ceramic Section, Mineral Processing Laboratory, Mineral Sciences Laboratories, CANMET, Energy, Mines and Resources Canada, Ottawa, K1A 0G1.

UNE ANALYSE ÉLECTROCHIMIQUE DES SYSTÈMES À ÉLECTROLYTE SOLIDE ET À ÉLECTRODE

J.D Canaday*, A.K. Kuriakose*, A. Ahmad* et T.A. Wheat*

Résumé

Les trois éléments constituants d'une pile que sont les gaz réactifs, les électrodes poreuses et l'électrolyte solide sont décrits en termes électrochimiques. Les processus associés à l'électrode qui causent le phénomène de la polarisation sont aussi discutés. L'utilisation des techniques à deux sondes et à trois sondes est présentée simultanément avec des exemples de résultats obtenus à partir de plusieurs systèmes.

*Chercheurs scientifiques, Section de la céramique, Laboratoire du traitement des minéraux, Laboratoires des sciences minérales, CANMET, Energie, Mines et Ressources, Ottawa, K1A 0G1.

CONTENTS

TABLES

FIGURES

1. INTRODUCTION

The Advanced Ceramic Materials Project is based, in part, on research and development activities in the area of beta-alumina and Nasicon-type materials (1). Ion-exchange methods (2) have extended the use of these ceramics to include functional ceramic devices such as sensors, gas pumps, fuel cells, and electrolyzers. Electrode studies (3,4) and electrochemical measurements (5) have also illustrated the industrial potential of these devices. In order to further assess the merits of these configurations, it is necessary to refine the electrochemical investigations of the electrolyte and electrode components.

The objective of this report is to provide a framework for the application of electrochemical principles to the CANMET three-phase system that utilizes gaseous reactants, porous metal electrodes, and a protonic (or cationic) solid electrolyte. The scope of this analysis is limited primarily to DC and transient methods, with a brief discussion of AC techniques.

2. THEORETICAL CONSIDERATIONS

2.1 CELL CONFIGURATIONS

Historically, electrochemical systems have been two-phase configurations with a liquid electrolyte and two metal electrodes (6). More recently, another two-phase configuration, a solid electrolyte with metal electrodes, has been investigated for use as a solid-state battery (7).

The introduction of gaseous reactants through porous electrodes for sensors and fuel cells has resulted in a three-phase system of gas, metal electrode, and liquid or solid electrolyte. The liquid system is exemplified by the KOH or H_3PO_4 fuel cell (8); ZrO_2 electrolytes have been used for oxygen sensors and high-temperature fuel cells (9). Solid protonic electrolytes have also been utilized in various electrochemical devices (10,11,12). A schematic diagram of these three cell types is shown in Figure 1.

2.2 THERMODYNAMIC PROPERTIES OF AN ELECTROCHEMICAL CELL

The phenomena associated with electrochemical cells can broadly be divided into two types. Thermodynamic effects occur under open-circuit conditions, while kinetic reactions leading to polarization processes result when an electrical current flows in a closed-circuit configuration. Thermodynamic effects have been considered by a number of authors (14,15,16), and their basic relations will be summarized here. For a hydrogen concentration cell with partial pressures, P_1 and P_2, the emf is given by:

$$V_{eq} = \frac{RT}{zF} \ln\left(\frac{P_1}{P_2}\right) \qquad \text{Eq 1}$$

where R is the gas constant, and T is the temperature. The term n represents the number of charges for the reaction $H_2 \rightarrow 2e^- + 2H^+$ (z = 2), and F is Faraday's constant, 96 485 Coulombs/mole. The free energy is

$$\Delta G = -nFV_{eq} \qquad \text{Eq 2}$$

or

$$\Delta G = -RT\ln K \qquad \text{Eq 3}$$

where K is the equilibrium constant.

The entropy is

$$\Delta S = \frac{\partial}{\partial T}\left(\Delta G\right)_P \qquad \text{Eq 4}$$

and the enthalpy is

$$\Delta H = \Delta G + T\Delta S \qquad \text{Eq 5}$$

or

$$\Delta H = nF\left[-V_{eq} + T\frac{\partial}{\partial T}\left(V_{eq}\right)_P\right] \qquad \text{Eq 6}$$

2.3 INTERFACE MODELS

An electrochemical interface is formed when an electrode is placed in contact with an

electrolyte. The electrode is primarily an electronic conductor, while the electrolyte is required to be an ionic conductor, as shown schematically (6,17) in Figure 2(a). This junction results in a double layer that can be modelled by a capacitance, C_{dl}, as seen in Figures 2(b) and 2(c). An ideally polarized interface is formed when the resistance of the equivalent circuit approaches infinity, as the capacitor charges up to the potential placed across the interface. When the resistance is zero, current leakage causes the interface to be ideally nonpolarized. Current-voltage curves for these ideal cases are shown in Figures 2(d) and 2(e).

2.4 ELECTRODE PROCESSES

The processes that occur at an electrochemical interface are numerous, complex, and interactive. They can be generally classified (17) as either faradaic or non-faradaic types. In the former case, charges are transferred across the interface in accordance with Faraday's Law (18):

$$J = \pm F J_m \qquad \text{Eq 7}$$

where the extent of the chemical reaction, symbolized by the molar flux density, J_m, is proportional to the electric current density represented by J. Faradaic processes are associated with the transfer of charge or mass. Charge-transfer reactions include oxidation, reduction, and ionization. Mass-transfer processes are due to the convection of gas through the cell gas flow system, diffusion through the porous electrode, and migration of ionic species through the electrolyte.

Under certain conditions, an interface will show a change of voltage when no charge transfer reactions occur because such reactions are thermodynamically or kinetically unfavourable (6). Here, processes such as adsorption or desorption can occur, and the structure of the interface can change with potential or with electrolyte composition. These processes are termed "non-faradaic".

These faradaic and non-faradaic processes are schematically shown in Figure 3(a) for a two-phase electrode/liquid-electrolyte reaction (17):

$$O + n\,e \rightleftharpoons R \qquad \text{Eq 8}$$

where O and R represent oxidized and reduced species. Similar concepts have been proposed for the two-phase electrode/solid-electrolyte interface (19).

A current density, J, is associated with an overpotential, η, which will be the sum of the overpotentials of each reaction,

$$\eta = \eta_{ct} + \eta_{mt} \qquad \text{Eq 9}$$

where η_{ct} and η_{mt} are the charge transfer (or activation polarization) and mass transfer (or concentration polarization) terms. The overall Faradaic electrode reaction can then be considered as a resistance, R_F, which is composed of a series of charge transfer and mass transfer steps such that

$$R_F = R_{ct} + R_{mt} \qquad \text{Eq 10}$$

A fast reaction is described by a small resistance, and a slow process is characterized by a large resistance. The slower step, which limits the overall electrode reaction, is called the "rate-determining step". An equivalent circuit of these mechanisms is shown in Figure 3(b).

2.5 POLARIZATION MECHANISMS

The operating voltage of an electrochemical cell, V_{cell}, is related (20) to the equilibrium potential, V_{eq}, and the polarization losses, V_p, by the equation

$$V_{cell} = V_{eq} \pm V_p \qquad \text{Eq 11}$$

The positive and negative signs apply when the cell is externally driven, as in the case of an electrolyzer, or when it functions in a self-driven manner as a fuel cell. Polarization of the electrodes results from charge transfer reactions or activation polarization, η_{act}, and from concentration polarization, η_{conc}, due to mass transfer processes. The electrolyte itself does not become polarized,

but an ohmic loss, η_{el}, occurs because of the IR resistance. Thus, the total polarization is the linear sum of these components:

$$V_p = \eta_{act} + \eta_{conc} + \eta_{el} \qquad \text{Eq 12}$$

Activation polarization is often modelled by the Butler-Volmer equation (6,17) for a one-step, single-electron transfer process as

$$J = J_o \left[\exp\left(\frac{\beta F \eta_a}{RT}\right) - \exp\left(\frac{-(1-\beta) F \eta_c}{RT}\right) \right] \qquad \text{Eq 13}$$

where η_a and η_c are the anodic and cathodic activation polarization terms.

The symmetry factors β and $(1-\beta)$ (6) are replaced by anodic and cathodic transfer coefficients, α_a and α_c, when multistep electrode reactions arise (21). A similar relation of the form

$$J = J_o' \left[\exp\left(\frac{e\eta}{kT}\right) - 1 \right] \qquad \text{Eq 14}$$

holds for a p-n semiconductor junction (6) and has been used to describe (22) silver and copper halides.

At large overpotentials, the Tafel form (17) of the Butler-Volmer equation results as

$$J = Jo \exp\left(\frac{\beta F \eta_a}{RT}\right) \qquad \text{Eq 15}$$

while for small values of the overpotential, expansion (17) of the exponential terms in Equation 13 gives the linear or "ohmic" relation

$$J = \frac{J_o F \eta_a}{RT} \qquad \text{Eq 16a}$$

The faradaic resistance is due to the charge transfer process, so that $R_F = R_{ct}$, and the exchange current density, Jo, can be evaluated from a plot of overpotential vs current density according to the relation

$$R_{ct} = \frac{\eta_a}{J} = \frac{RT}{FJ_o} \qquad \text{Eq 16b}$$

The ohmic loss due to the electrolyte is included in the term, V_p, and is represented as

$$\eta_{el} = IR = JAR = \rho LJ \qquad \text{Eq 17}$$

Here, the terms A, ρ, and L are the cross-sectional area, resistivity, and thickness of the electrolyte.

When Fick's law of diffusion is applied to the electrode reactant species (8), the concentration polarization is given by

$$\eta_{conc} = \frac{RT}{nF} \ln \frac{J_L}{J_L - J} \qquad \text{Eq 18}$$

where J_L is the limiting current density.

It is instructive to consider in further detail the various processes by which material is transported to, and away from, the electrochemical interface, since it is these phenomena that result in concentration polarization of the electrodes and in ohmic polarization of the electrolyte.

For a single liquid phase, the general equation (17) for the molar flux of a species in one dimension is

$$j = C v - \frac{D \, dC}{dx} - \frac{zF}{RT} D C \frac{dV}{dx} \qquad \text{Eq 19}$$

where the terms represent convection, diffusion, and migration, respectively. The concentration of the species is given by C, the linear velocity is v, and the diffusion coefficient is D. Diffusion and migration are caused by the concentration and potential gradients, dC/dx and dV/dx.

Figure 4 illustrates the mass transfer mechanisms for the three-phase solid protonic electrolyte system. The ideal-gas law gives a molar concentration of

$$\eta_m = \frac{N}{V} = \frac{P}{RT} \qquad \text{Eq 20}$$

and the gas flow rate for the convective term is

$$f = vA \qquad \text{Eq 21}$$

where A is the cross-sectional area. Thus, the molar flux due to ideal-gas convection is

$$J_f = \frac{P}{RT}\frac{f}{A} \qquad \text{Eq 22}$$

The limiting molar flux of an ideal gas diffusing through a porous electrode of porosity, p, and tortuosity, τ, is given by (10,23)

$$J_{L,m} = \frac{D_g}{RT}\frac{dP}{dx}\frac{p}{\tau} \qquad \text{Eq 23}$$

Ionic species will migrate through the electrolyte under the influence of an electric field, E = dV/dx, so that the molar flux of these ions will be

$$J_b = \frac{zF}{RT} D_b C \frac{dV}{dx} \qquad \text{Eq 24}$$

where D_b is the bulk diffusion coefficient. Equation 24 is another form of Ohm's Law, in which the mobility of the charged species is

$$\mu = \frac{zF}{RT} D, \qquad \text{Eq 25}$$

so that the current density of ionic transport in the electrolyte is

$$J_b = q\mu\eta_e E \qquad \text{Eq 26}$$

where the conductivity is $\sigma = q\mu\eta_e$ and η_e is the number of charges per cm^3.

Calculated values of molar flux density and electric current density due to convection, diffusion, and migration are given in Table I. The convective transport relation assumes a flow of hydrogen gas with P = 1 atm, T = 100°C, f = 100 $cm^3 min^{-1}$, and A = 1 cm^2. The limiting flux density due to the self-diffusion (25) of hydrogen through an electrode is calculated for a thickness dx = 10 μm, a ratio of porosity to tortuosity of $p/\tau = 0.1$, a pressure drop of dP = 1 atm, and a diffusion coefficient $D_g = 2.0\ cm^2\ s^{-1}$ as calculated from Equation 21. Migration of ions through the electrolyte assumes a conductivity of $\sigma = 10^{-3}\ (ohm\text{-}cm)^{-1}$ and an electric field of dV/dx = 1 volt/0.1 cm.

It can be clearly seen from Table I that the limiting mass-transfer process is due to the migration of charged species in the electrolyte. While not a polarization process itself, since it does not occur in the electrodes, this mechanism is often referred to as "Ohmic polarization" because of the nature of this transport phenomenon.

2.6 CAPACITIVE EFFECTS

For hydrogen-conducting solid electrolytes, only a small amount of impedance data have been reported (26). Interfacial measurements of oxygen-conductors have shown the presence of adsorbed neutral atoms at the gas-electrolyte interface (18), and these capacitances have been found to be related to the oxygen partial pressure by $P(O_2)^{-1/2}$. The electrode capacitance was given by

$$C = \frac{2F^2 \Theta S}{RT} \qquad \text{Eq 27}$$

where Θ is a fraction of the surface covered, and S is the number of possible adsorption sites. This determination of capacitance did not distinguish between the adsorption effects of the metal electrode or the electrolyte, but it was believed that both were likely to be adsorbants. In both cases, the sequence of events was thought to be dissociative adsorption on the solid surface followed by a rapid diffusion toward the triple-phase line, and then the electrochemical reaction. The capacitive effects due to space-charge polarization have been discussed in detail (27) and will not be considered here.

2.7 ELECTRODE MORPHOLOGY

The morphology of the electrodes for two-phase systems is relatively simple, whether the electrolyte is of the liquid- or solid-state type. These electrodes consist of metal sheets, and the interfaces are, in geometrical terms, well defined. For three-phase systems,

it is not only the charge-transfer and mass-transfer faradaic processes that contribute to the polarization of the electrode, but also its morphological characteristics (28).

The cathode of the ZrO_2 cell has been extensively studied (23) in terms of structure and the effect of various morphologies on electrode reactions.

In the case of solid protonic three-phase systems, analyses of electrode materials (3), morphological properties (4), gas-phase relations (29), and polarization processes (25) have been made. In addition to these studies, experiments (30) are under way to measure thick-film electrode structural parameters such as porosity, surface area, and three-phase line.

The morphology of a porous electrode on a solid electrolyte has been observed to consist of five regions (18):

- a porous region that allows mass transfer by gaseous diffusion;
- electrode bulk material that allows transport by diffusion of absorbed material;
- electrode surface where surface diffusion or catalysis occurs;
- electrolyte surface where electronic, molecular, atomic, or ionic diffusion may take place;
- electrolyte bulk that allows ionic diffusion from electric fields and concentration gradients.

These regions and the transport paths are illustrated in Figure 5 for a three-phase system.

The processes in each of these five regions interact, making a precise analysis impossible. However, it should be feasible to identify the slowest or rate-determining step of the overall electrode reaction. For example, three reactions may occur at the anode (18):

- supply of neutral chemical species and dissociation;
- oxidation or reduction (electron transfer);
- transfer of ionic species across the electrode-electrolyte interface.

These reactions may be symbolized by the following equations:

$$H_2 \rightarrow H + H \qquad \text{Eq 28}$$

$$H \rightarrow H^+ + e^- \qquad \text{Eq 29}$$

$$H^+_{electrode} \rightarrow H^+_{electrolyte} \qquad \text{Eq 30}$$

General electrode processes for three-phase systems are given in Table 2.

2.8 CRITERIA FOR REFERENCE ELECTRODES

An electrochemical cell can be described in terms of two properties (31). Thermodynamic phenomena arise when the cell is at equilibrium under the open-circuit condition. As seen in Section 2.2, the equilibrium cell potential develops because of charge separation at the interfaces. Measurement of V_{eq} and dV_{eq}/dT permits a determination of ΔG, ΔH, ΔS, and K for the cell reaction. The electrode where the activity ratio is known is the reference electrode. Kinetic phenomena result when the cell is operated under the closed-circuit, non-equilibrium condition. This property is the result of the various faradaic and non-faradaic processes that occur in the cell. In this case, three electrodes can be used. Two- and three-probe cells are shown in Figure 6.

The addition of a third probe, the reference electrode, allows for both a reduction in the electrolyte resistance and for a distinction between anodic and cathodic polarization effects. The electrode of interest to which an

external current or voltage is applied is called the working electrode (WE). Its potential is measured relative to that of the reference electrode (RE). Current is passed between the working electrode and the counter electrode (CE).

For liquid electrolytes, the accepted primary reference is the standard or normal hydrogen electrode (17) containing components of unit activity,

$$Pt \left| H_2 \ (a = 1) \right| H + (a = 1, \text{aqueous}).$$

A more common reference is the saturated calomel electrode,

$$Hg \left| Hg_2 Cl_2 \right| KCl \ (\text{saturated})$$

with a potential of 0.242 volts relative to the standard hydrogen electrode.

Because the reference electrode has a constant composition, its potential is fixed; changes in the cell potential are due to the working electrode. Thus, a good reference electrode must approach an ideal nonpolarizable (or nonblocking) electrode as illustrated in Figure 2, in which the passage of current does not change its potential.

The type of reference used with liquid electrolytes also depends on the application. Thermodynamic measurements made under open-circuit conditions require a higher degree of precision than those used for kinetic studies, because it is the change in potential rather than its absolute value that is important. Criteria (32) for liquid-electrolyte reference electrodes include (1) a high exchange-current density (i.e., nonpolarizability); (2) a variation of potential with concentration (activity) according to the Nernst equation; (3) reproducibility and stability of potential; and (4) a fast response.

The properties of reference electrodes for two-phase and three-phase solid electrolyte systems have also been considered (33). Here, a number of three-probe configurations with wire-probe reference electrodes were discussed. It was found that the interfacial impedance, accounting for both faradaic and non-faradaic processes, must be small enough that the reference electrode maintains a constant potential difference with respect to the electrolyte. It was also emphasized that achieving equilibrium for solid-electrolyte three-phase systems is much more difficult than for aqueous-electrolyte two-phase systems.

Two-probe emf measurements of three-phase solid electrolyte systems have been described. Reversibility of all electrode processes, with minimum polarization under the measurement conditions, was found to be the primary consideration in the selection of reference electrodes (34). The necessity of establishing separately the degree of reversibility for charge transfer (activation polarization) and mass transfer (concentration polarization) effects was also suggested. Electrodes in equilibrium with appropriate reference gases were discussed (35,36) for thermodynamic measurements.

3. EXPERIMENTAL METHODS

3.1 ELECTRODE GEOMETRY

Figure 7 illustrates a number of electrode configurations that have been used in the investigation of zirconia and protonic three-phase systems.

In most cases, the emphasis of these studies was on kinetic measurements. Figure 7(a) shows a two-probe sample (37,38,39) in which the Pt reference electrode was the counter electrode for the zirconia electrolyte. The cell (anode plus cathode) overpotential was calculated from the relation

$$\eta = V - IR - V_{eq} \qquad \text{Eq 31}$$

In Figure 7(b), the reference electrode was a ceramic material in contact with a zirconia electrolyte (40). Platinum was sputtered on zirconia to produce the configuration shown (41) in Figure 7(c), where the area of the reference electrode was minimized. A platinum paste reference electrode located on the same

side of the zirconia electrolyte as the working electrode was prepared (28,42) for steady-state, transient, and impedance measurements; this arrangement appears in Figure 7(d).

A system containing two reference electrodes has also been reported (21), and is shown in Figure 7(e). The overpotential of each working electrode was determined from the relation

$$\eta = V - 0.5\ IR_b - V_o \qquad \text{Eq 32}$$

where V and V_o were the potential differences between the working and reference electrodes at currents of I and I = 0, respectively. The term IR_b was the ohmic loss due to the electrolyte as measured with an impedance bridge at 1 kHz, and the factor of 0.5 resulted from the symmetry of the electrode arrangement.

To avoid the difficulties associated with reproducibility of results from electrodes of various morphological characteristics, a point probe (43) was chosen as a working electrode for the cell shown in Figure 7(f).

Both zirconia and protonic cells (33,44) have been studied using a wire probe inserted into the electrolyte as a reference electrode; this design is illustrated in Figure 7(g).

Arrangements similar in concept to that shown in Figure 7(g) are the configurations of Figures 7(h) and (i) (45,46), where a concentric wire and Ag epoxy, respectively, were utilized as reference electrodes.

An arrangement that maximizes the current density of the working electrode relative to that of the counter electrode (47) is shown in Figure 7(j).

3.2 EQUIVALENT CIRCUITS FOR CELLS

Equivalent circuits for two- and three-probe electrochemical cells are shown in Figure 8. The terms R_a and R_c represent the faradaic processes of charge transfer and mass transfer occurring at the anode and cathode. Non-faradaic mechanisms such as adsorption are symbolized by capacitances, C_a and C_c. The resistance of the bulk electrolyte is given by R_b. Detailed impedance analyses of the solid-electrolyte/electrode interface have been developed by a number of researchers (27,48,49).

3.3 INSTRUMENTATION AND MEASUREMENT TECHNIQUES

In order to understand the processes that occur in electrochemical cells, a number of steady-state and transient experiments can be performed.

Steady-state, DC techniques include cell discharge, the application of external current or voltage, and potentiostatic-galvanostatic experiments.

These measurement methods are shown collectively with the equivalent circuit of Figure 8 in Figure 9. An automated system for measuring the cell (50) is shown in Figure 10. For an internally driven cell such as a battery or a fuel cell, a load resistor, R_c, is placed in parallel with the cell, and the cell is allowed to discharge. An example of this two-probe result is shown in Figure 11 (51). This discharge curve is of the form

$$V_{cell} = V_{eq} - (\eta_a + \eta_c + IR_b) \qquad \text{Eq 33}$$

where the polarization terms η_a, η_c, and IR_b are caused by processes at the anode, cathode, and within the electrolyte. Here, the anodic and cathodic overpotentials cannot be separated; their sum, the cell overpotential, is measured as

$$\eta_{cell} = \eta_a + \eta_c \qquad \text{Eq 34}$$

When the cell is externally driven, the cell overpotential can be determined from the relation

$$V_{ap} = V_{cell} = V_{eq} + \eta_{cell} + IR_b \qquad \text{Eq 35}$$

As is the case for an internally driven cell, only the total cell overpotential can be found with this two-probe technique.

When it is required that the electrode overpotentials be known separately, a three-probe potentiostat/galvanostat can be utilized. With the potentiostatic method, a current is forced between the counter and working electrodes to maintain the desired potential of the working electrode relative to the reference electrode. With the introduction of a reference electrode, the electrolyte resistance, R_b, is divided into two components, R_u and R', where R_u is the uncompensated resistance between the reference electrode and the interfacial impedance at the working electrode. Between the reference electrode and the counter electrode, there remains an electrolyte resistive component, R'. Potentiostatic techniques for IR compensation are available (52,53) for minimizing this contribution.

An alternative means of separating the overpotential of the working electrode from the uncompensated electrolyte resistance is the use of the current-interruption technique. This method has been used in the investigation of the oxygen-ion conductor, CeO_2 (28). Because of the difference in the chemical potential of the mobile ionic species between the electrolyte and the electrode, the charge carriers on both sides of the interface will redistribute themselves along the boundary to form a double layer. Application of a constant current (Fig. 12(a)) from time t_o to t_1 charges the double layer capacitance. Following the interruption of this current, the overpotential decays as the double layer discharges according to the relation

$$I(t) = -C_{d\eta} \frac{d\eta(t)}{dt} \qquad \text{Eq 36}$$

The time dependence of the overpotential is observed on an oscilloscope as schematically shown in Figure 12(b).

The rapid decrease in the measured potential is due to uncompensated resistance of the electrolyte, IR_u, which occurs in a time of $\sim 10^{-7}$ sec. An equivalent circuit of this interface is shown in Figure 11(c). The initial value of the measured potential after the IR_u drop is the steady-state overpotential, $\eta(o)$, corresponding to the applied current, $I_{ap} = I(o)$, which flows just prior to the interruption. It is these values of $\eta(o)$ and I(o) that are related by the steady-state charge-transfer polarization process, according to the Butler-Volmer equation

$$I(o) = I_o\left[\exp\left(\frac{\alpha_a e\eta(o)}{kT}\right) - \exp\left(\frac{-\alpha_c e\eta(o)}{kT}\right)\right] \qquad \text{Eq 37}$$

where α_a and α_c are the anodic and cathodic transfer coefficients.

3.4 FOUR-PROBE TECHNIQUE

An additional method, which is used in determining the DC conductivity of thin film electrode and bulk electrolyte material, is the four-probe technique. A schematic diagram of the experimental arrangement appears in Figure 13.

This configuration eliminates the polarization effects that may occur at the electrode-electrolyte interfaces. Theoretical aspects (54) and geometrical correction factors (55) for this method have also been considered. For an infinitely thick sample, the resistivity is given by

$$\rho = 2\pi a \frac{V}{I} \qquad \text{Eq 38}$$

while for a thin sample, the resistivity is

$$\rho = \frac{\pi t}{\ln 2} \frac{V}{I} \qquad \text{Eq 39}$$

and the sheet resistance is

$$R_s = \frac{\rho}{t} = 4.53 \frac{V}{I} \qquad \text{Eq 40}$$

A summary of the two-, three-, and four-probe techniques for thermodynamic and kinetic measurements is given in Table 3. The measured quantities and the separation of these terms into their components are also shown.

4. DISCUSSION OF THREE-PHASE SYSTEMS

The three-phase system with zirconia or protonic-type electrolytes has been measured using two-probe and three-probe devices. Two-probe techniques include the discharge of an internally driven cell and the application of

an externally applied DC voltage or current. Potentiostatic-galvanostatic and current interruption instruments have been used as three-probe devices. In this section, the results of some of these studies will be reviewed.

Plots of anodic and cathodic overpotential vs log I, as obtained by the current-interrupt method for CeO_2 (28), are shown in Figures 14(a) and 14(b). The data were fitted by the Butler-Volmer equation with $\alpha_a = \alpha_c = 1$. These results demonstrated that electrode polarization at both the anode and the cathode was controlled by a charge-transfer process at high partial pressures of oxygen. Concentration polarization resulted when the cathode was exposed to low oxygen partial pressure.

The current-interruption method has also been applied (56) to the investigation of polarization effects where the electrolyte was a protonic $SrCeO_3$ material. The major limitation of the cell was found to be the ohmic resistance of the electrolyte, while the anodic polarization was seen to have a negligible effect. Cathodic polarization was measured for a number of oxygen partial pressures. The dependence of the polarization resistance on the oxygen partial pressure, $R_p \alpha P_{O_2}^{-1/4}$, suggested that the rate-determining step for the cathode reaction was the surface diffusion of adsorbed oxygen atoms on the platinum electrode to the electrochemically active site of the electrolyte.

Cell performance and electrode polarization (45), as determined by two- and three-probe discharge measurements for the protonic conductor, $SrCeO_3$, are shown in Figures 15(a) and (b). The total cell resistance as found from Figure 15(a) was $\simeq$ 10 ohms. Anodic polarization was negligible, as seen in Figure 15(b), while some cathodic polarization was present.

5. SUMMARY AND CONCLUSION

Two-phase electrochemical cells with liquid and solid electrolytes have been described. These two systems have also been compared to the more complex three-phase system that is the cell of primary interest in the CANMET Advanced Ceramic Materials Project.

Two-probe measurements were found to be required when determining the thermodynamic properties of the cell. The two-probe technique was also useful for the measurement of overall cell performance when the separation of anodic, cathodic, and electrolyte polarization factors was not required.

A three-probe configuration was shown to be necessary for the measurement of kinetic properties when knowledge of the polarization components was required. The reference electrode caused the solid electrolyte to act as a voltage divider with the uncompensated resistance located between the reference electrode and the interfacial impedance of the working electrode; a second resistive component of the electrolyte remained between the reference electrode and the counter electrode. The uncompensated portion of the electrolyte resistance could be reduced or eliminated by potentiostatic compensation methods. This component could also be separated from the working electrode overpotential by the current-interruption method. The electrode geometry of the three-electrode configuration was not an important factor in determining the electrode polarization if elimination or separation of the uncompensated electrolyte resistance could be achieved.

Electrode morphological characteristics of the three-phase system were also seen to affect the cell's polarization mechanisms.

Application of these two-probe and three-probe methods has resulted in the determination of fundamental quantities for three-phase oxygen-ion and protonic solid electrolyte cells. Their use with hydrogen-conducting Nasicon and beta-alumina will enhance the understanding of these materials and their role in electrochemical cells.

6. REFERENCES

1. Wheat, T.A.; Ahmad, A.; and Kuriakose, A.K., Editors. "Progress in solid electrolytes"; *Division Report* ERP/MSL 83-94(TR); CANMET, Energy, Mines and Resources Canada; 1983.

2. Kuriakose, A.K.; Wheat, T.A.; Ahmad, A.; and Canaday, J.D. "A new method for the fabrication of polycrystalline hydrogen-conducting solid electrolytes"; *Division Report* ERP/MSL 85-149(IR); CANMET, Energy, Mines and Resources Canada; 1985.

3. Canaday, J.D.; Kuriakose, A.K.; Ahmad, A.; and Wheat, T.A. "Electrode materials for protonically conducting solid electrolyte fuel cells"; *Division Report* ERP/MSL 83-120(IR); CANMET, Energy, Mines and Resources Canada; 1983.

4. Canaday, J.D.; Kuriakose, A.K.; Ahmad, A; and Wheat, T.A. "Electrodes for solid-state electrolyte fuel cells - electrode morphology"; *Division Report* ERP/MSL 83-134(IR); CANMET, Energy, Mines and Resources Canada; 1983.

5. Canaday, J.D.; Kuriakose, A.K.; Ahmad, A.; and Wheat, T.A. "Electrical measurements of protonic solid electrolyte cells"; *Division Report* ERP/MSL 86-27(OP); CANMET, Energy, Mines and Resources Canada; 1986.

6. Bockris, J.O.M., and Reddy, A.K.N. *Modern Electrochemistry*, Volumes 1 and 2; Plenum Press; New York; 1970.

7. Jensen, J. "Electrolytes for all-state lithium batteries and hydrogen fuel cells"; *Progress in Solid Electrolytes*; T.A. Wheat, A. Ahmad, and A.K. Kuriakose, Editors; Energy, Mines and Resources, Canada; 1983.

8. McDougall, A. *Fuel Cells*; John Wiley & Sons; New York; 1976.

9. Subbarao, E.C., Editor. *Solid Electrolytes and Their Applications*; Plenum Press; New York; 1980.

10. Jensen, J., and Kleitz, M. *Solid State Protonic Conductors I*; Odense University Press; Odense, Denmark; 1982.

11. Goodenough, J.B.; Jensen, J; and Kleitz, M. *Solid State Protonic Conductors II*; Odense University Press; Odense, Denmark; 1983.

12. Goodenough, J.B.; Jensen, J.; and Kleitz, M. *Solid State Protonic Conductors III*; Odense University Press; Odense, Denmark; 1985.

13. Gould, R.G., Editor. *Advances in Chemistry Series*; American Chemical Society; Washington, D.C.; 1969.

14. Young, G.J. *Fuel Cells*; Reinhold Publishing Corp.; New York; 1963.

15. Austin, L.G. "The electrochemical theory of fuel cells"; *Handbook of Fuel Cell Technology*; C. Berger, Editor; Prentice Hall Inc.; Englewood Cliffs, N.J.; 1968.

16. Oniciu, L. *Fuel Cells*; Abacus Press; Kent, England; 1976.

17. Bard, A.J., and Faulkner, L.R. *Electrochemical Methods*; John Wiley & Sons; New York; 1980.

18. Schouler, E.J.L.; Birchall, M.L.S.; and Lundsgaard, J.S. "Porous electrodes for solid electrolyte systems"; *Solid State Protonic Conductors I*; Odense University Press; Odense, Denmark; 1982.

19. Vedel, J. "Electrode reactions at electrode-solid electrolyte interfaces. Use of electroanalytical techniques"; *Electrode Processes in Solid Ionics*; M. Kleitz and J. Dupuy, Editors; D. Reidel Publishing Co.; Dordrecht, Holland; 1976.

20. Steele, B.C.H. "High temperature fuel cells and electrolysers"; *Electrode Processes in Solid Ionics*; M. Kleitz, and J. Dupuy, Editors; D. Reidel Publishing Co.; Dordrecht, Holland; 1976.

21. Ong, B.G.; Chiang, C.C.; and Mason, D.M. "Electrocatalytic role of stabilized zirconia on the anodic current - overpotential behavior in hydrocarbon fuel cells"; *Solid State Ionics* 3/4:447; 1981.

22. Wagner, J.B. "Polarization studies on solid state electrolytes"; *Electrode Processes in Solid State Ionics*; M. Kleitz and J. Dupuy, Editors; D. Reidel Publishing Co.; Dordrecht, Holland; 1976.

23. Pizzini, S.; Bianchi, M.; Colombo, P.; and Torchio, S. "On the influence of the annealing temperature and heavy current treatments on the porous structure of platinum electrodes and on the kinetics of the oxygen reaction at high temperatures"; *J Appl Electrochem* 3:153; 1973.

24. Sze, S.M. *Physics of Semiconductor Devices*; Wiley-Interscience; New York; 1969.

25. Canaday, J.D.; Wheat, T.A.; Kuriakose, A.K.; and Ahmad, A. "A polarization model for protonic solid electrolyte fuel cells"; *Division Report* ERP/MSL 84-157(OP&J); CANMET, Energy, Mines and Resources Canada; 1984.

26. Schouler, E.J.L. "Impedance spectroscopy in solid state electrochemistry"; *Solid State Protonic Conditions III*; J.B. Goodenough, J. Jensen, and A. Potier, Editors; Odense University Press; Odense, Denmark; 1985.

27. Macdonald, J.R. "Space charge polarisation"; *Electrode Processes in Solid Ionics*; M. Kleitz and J. Dupuy, Editors; D. Reidel Publishing Co.; Dordrecht, Holland; 1976.

28. Wang, D.Y., and Nowick, A.S. "Cathodic and anodic polarization phenomena at platinum electrodes with doped CeO_2 as electrolyte. I. Steady-state overpotential"; *J Electrochem Soc* 126:1155; 1979.

29. Canaday, J.D.; Wheat, T.A.; Ahmad, A.; and Kuriakose, A.K. "Gas phase relations for protonic solid-electrolyte fuel cells"; Accepted for publication in the *J Appl Electrochem*; 1986.

30. Department of Supply and Services Contract No. 03SP.23440-4-9223. *Characterization of Thin Films Used as Electrodes in Electrochemical Devices*; Ontario Research Foundation (to be completed Dec. 1986 or first part of 1987).

31. Smith, D.E. "Thermodynamic and kinetic properties of the electrochemical cell"; *J Chem Educ* 60:299; 1983.

32. Gileadi, E.; Kirowa-Eisner, E.; and Penciner, J. *Interfacial Electrochemistry*; Addison-Wesley Publishing Company; Inc.; Reading, Mass.; 1975.

33. Bottelberghs, P.H. "Low frequency measurements on solid electrolytes and their interpretations"; *Solid Electrolytes*; P. Hagenmuller and W. Van Gool, Editors; Academic Press; New York; 1978.

34. Chandrasekharaiah, M.S.; Sreedharan, O.M.; and Chattopadhyay, G. "Thermodynamic studies of alloys and intermetallic compounds"; *Solid Electrolytes and their Applications*; E.C. Subbarao, Edi- tor; Plenum Press; New York; 1980.

35. Seetharaman, S., and Abraham, K.P. "Thermodynamic properties of oxide systems"; *Solid Electrolytes and their Applications*; E.C. Subbarao, Editor; Plenum Press; New York; 1980.

36. Jagannathan, K.P.; Tiku, S.K.; Ray, H.S.; Ghosh, A.; and Subbarao, E.C. "Technological applications of solid electrolytes"; *Solid Electrolytes and their Applications*; E.C. Subbarao, Editor; Plenum Press, New York; 1980.

37. Etsell, T.H., and Flengas, S.N. "Over-potential behavior of stabilized zirconia solid electrolyte fuel cells"; *J Electrochem Soc* 118:1890; 1971.

38. Gur, T.M.; Raistrick, I.D.; and Huggins, R.A. "Steady-state d.c. polarization characteristics of the oxygen platinum/stabilized zirconia interface"; *J Electrochem Soc* 127:2620; 1980.

39. Verkerk, M.J.; Hammink, M.W.J.; and Burggraaf, A.J. "Oxygen transfer on substituted ZrO_2, Bi_2O_3, and CeO_2 electrolytes with platinum electrodes"; *J Electrochem Soc* 130:70; 1983.

40. Badwal, S.P.S.; Bevan, D.J.M.; and Bockris, J.O.M. "The electrode kinetics of the evolution and dissolution of oxygen at the urania-zirconia interfaces"; *Electrochemica Acta*; 25:1115; 1980.

41. Winnubst, A.J.A.; Scharenborg, A.H.A.; and Burgraat, A.J. "The electrode resistance of ZrO_2 - Y_2O_3 (Bi_2O_3) solid electrolytes with Pt electrodes"; *Solid State Ionics* 14:319; 1984.

42. Wang, D.Y., and Nowick, A.S. "Cathodic and anodic polarization phenomena at platinum electrodes with doped CeO_2 as electrolyte. II. Transient overpotential and A.C. impedance"; *J Electrochem Soc* 126:1166; 1979.

43. Olmer, L.J., and Isaas, H.S. "The effect of electrode surface impurities on the oxygen electrode reaction at zirconia electrolytes"; *J Electrochem Soc* 129: 345; 1982.

44. Nakamura, O., and Ogino, I. "Three-electrode solid state fuel cell for evaluating working electrodes"; *Solid State Ionics* 6:337; 1982.

45. Iwahara, H.; Uchida, H.; and Tanaka, S. "High temperature proton conductor based on $SrCeO_3$ and its application to solid electrolyte fuel cells"; *Solid State Ionics* 9/10:1021; 1983.

46. Canaday, J.D. Unpublished experimental electrode configuration, 1986.

47. Pizzini, S.; Bianchi, M.; Corradi, A.; and Mari, C. "Influence of cell geometry on the shape of polarization curves of porous platinum electrodes on a YSZ electrolyte"; *J Appl Electrochem* 4:7; 1974.

48. Armstrong, R.D. "Impedance diagrams for solid electrolyte cells"; *Electrode Processes in Solid State Ionics*; M. Kleitz and J. Dupuy, Editors; D. Reidel Publishing Co.; Dordrecht, Holland; 1976.

49. Ahmad, A.; Canaday, J.D.; Wheat, T.A.; and Kuriakose, A.K. "A computer controlled data acquisition system for electrical/electrochemical characterization of ceramic materials"; *J Can Ceramic Soc* 53:8; 1984.

50. Canaday, J.D.; Wheat, T.A.; Kuriakose, A.K.; and Ahmad, A. "A microcomputer system for fuel cell measurements"; Presented at the Spring 1985 Meeting of the Electrochemical Society; Toronto, Canada.

51. Canaday, J.D. Unpublished data; 1986.

52. Gileadi, E.; Kirowa-Eisner, E.; and Penciner, J. *Interfacial Electrochemistry, an Experimental Approach*; Addison-Wesley Publishing Co., Inc.; Reading, Mass; 1975.

53. Macdonald, D.D. *Transient Techniques in Electrochemistry*; Plenum Press; New York; 1977.

54. Van der Pauw, L.J. "A method of measuring specific resistance and Hall Effect of discs of arbitrary shape"; *Phillips Res Reports* 13:1; 1958.

55. Valdes, L. "Resistivity measurements on germanium for transistors"; *Proc I.R.E.* 42:420; 1954.

56. Uchida, H.; Tanaka, S.; and Iwahara, H. "Polarization of Pt electrodes of a fuel cell with a high temperature-type proton conductive solid electrolyte"; *J Appl Electrochem* 15:93; 1985.

TABLES

Table 1 - Comparison of molar flux density and current density for the convection, diffusion, and migration processes

	Convection	Diffusion Fick's Law	Migration Ohm's Law
Molar flux density $\frac{\text{moles}}{\text{cm}^2 \text{ sec}}$	1.0×10^{-4}	8.0×10^{-4}	1.0×10^{-7}
Current density $\frac{\text{A}}{\text{c m}^2}$	10	80	1.0×10^{-2}

Table 2 - Electrode processes for ceramic electrolyte three-phase systems

Faradaic processes

Charge transfer
- oxidation
- reduction

Mass transfer
- convection of reactant gas species through gas flow system
- diffusion of reactant gas species through porous electrodes
- surface diffusion of reactant gas species on electrodes or electrolyte
- migration of ionic species through electrolyte

Non-faradaic processes

Chemical reactions
Molecular dissociation
Capacitive effects
- adsorption-desorption
- space charge

Table 3 - Summary of measurement techniques for thermodynamic and kinetic properties

Property	Measurement techniques: Two-probe	Three-probe	Four-probe
Thermodynamic	Measure V_{eq}, T, P Gives ΔG, K, ΔS, ΔH	Not applicable	Not applicable
Kinetic	Measure I and $\eta_a + \eta_c + IR_b$ where $\eta_{cell} = \eta_a + \eta_c$ Separates η_{cell} and IR_b with two-probe AC impedance measurement or four-probe DC measurement of bulk electrolyte	Measure I and $\eta_a(o) + IR_u$ or $\eta_c(o) + IR'_u$ Separates $\eta_a(o)$ and η_c (o) Separates $\eta_a(o)$ and IR_u or $\eta_c(o)$ and IR'_u with current interruption or potentiostatic IR_u compensation	Measure I and V Eliminates η_a and η_c
	Gives cell performance	Gives polarization mechanism of each electrode	Gives R_b and ρ of bulk electolyte or R_s of thin-film electrode

FIGURES

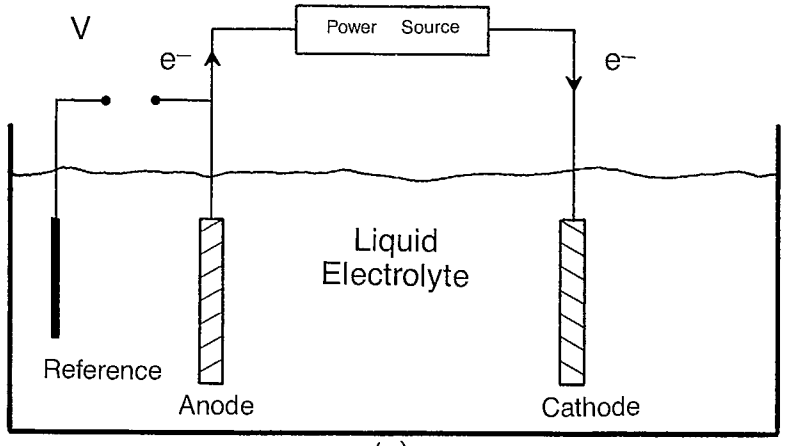

Non-porous Electrodes

(a)

Two-phase liquid electrolyte system

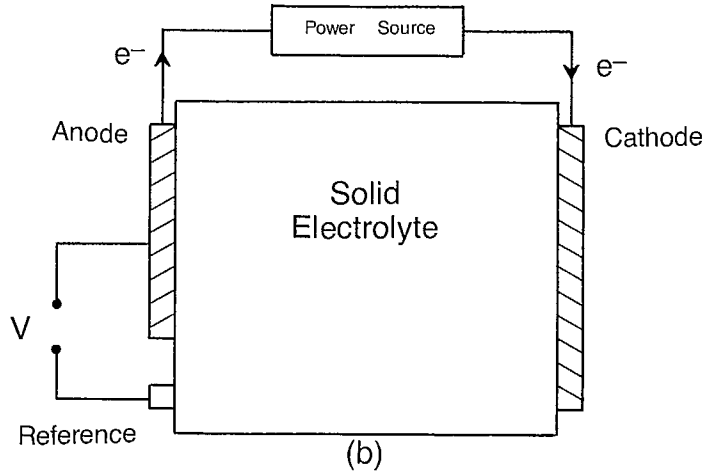

Non-porous Electrodes

(b)

Two-phase solid electrolyte system

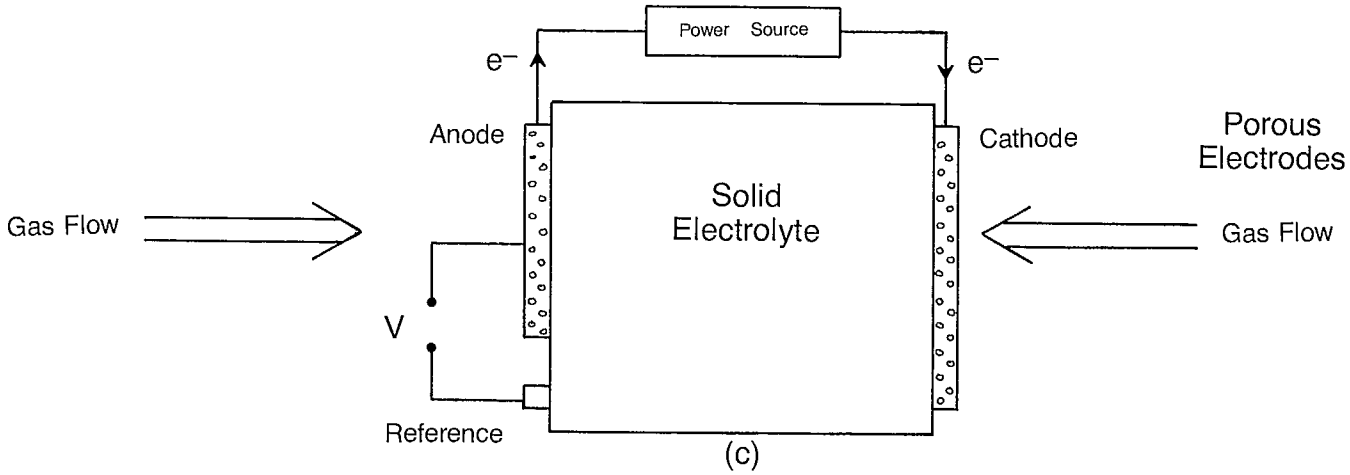

(c)

Three-phase solid electrolyte system

Fig. 1 - Schematic diagram of three types of electrochemical cells

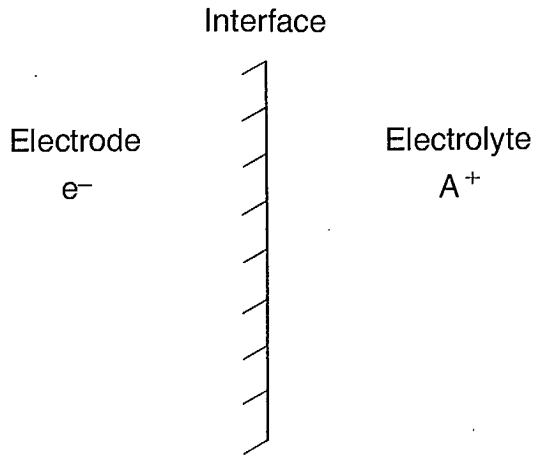

(a)
Model of an ideal interface

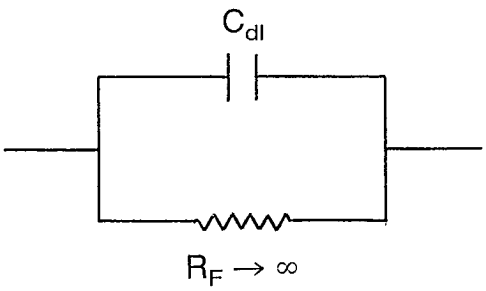

(b)
Equivalent circuit of an ideally polarized interface

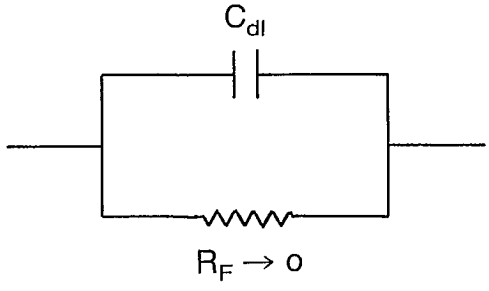

(c)
Equivalent circuit of an ideally non-polarized interface

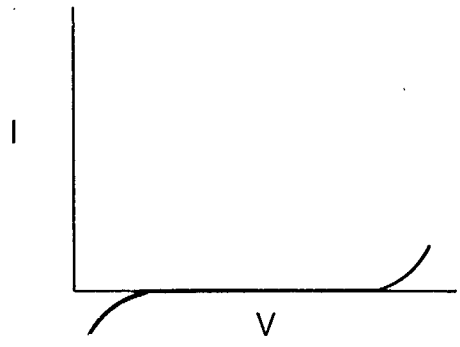

(d)
Current-voltage curve for an ideally polarized interface

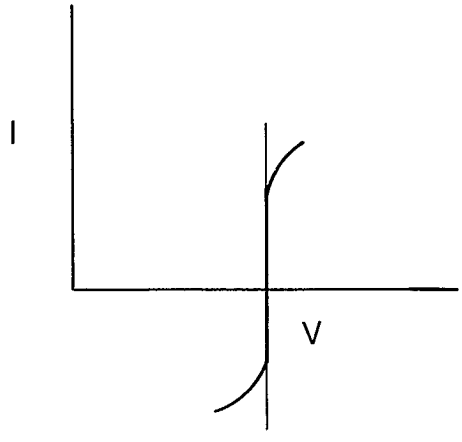

(e)
Current-voltage curve for an ideally non-polarized interface

Fig. 2 - Electrochemical interface model

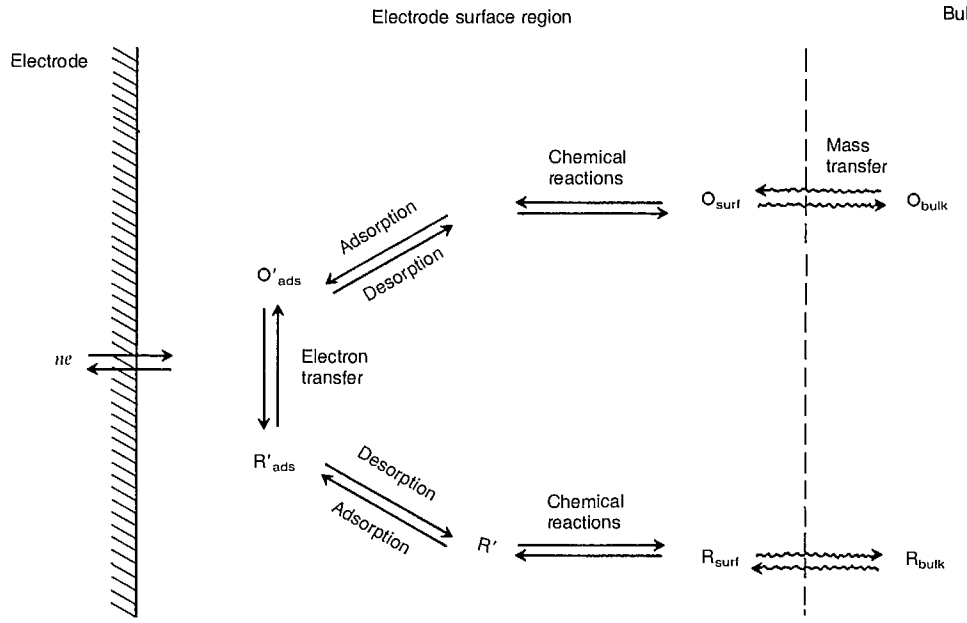

(a)

Electrode reactions (Ref 17)

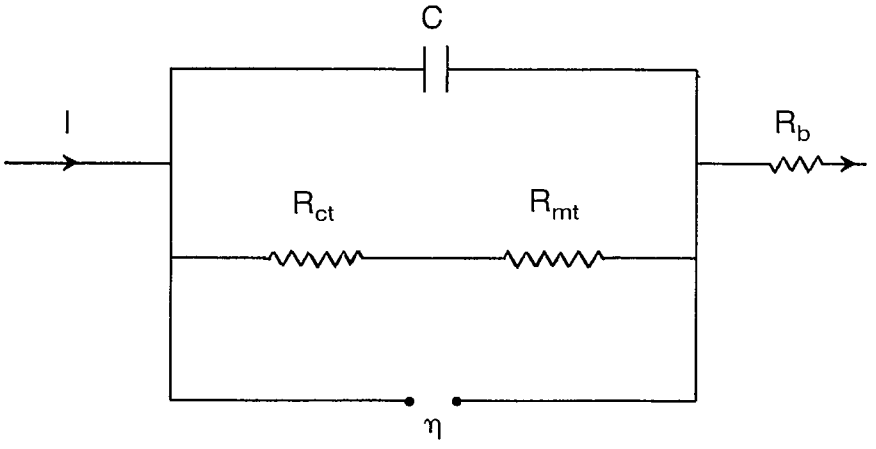

(b)

Equivalent circuit

Fig. 3 - Electrochemical processes for a two-phase electrode/liquid-electrolyte system

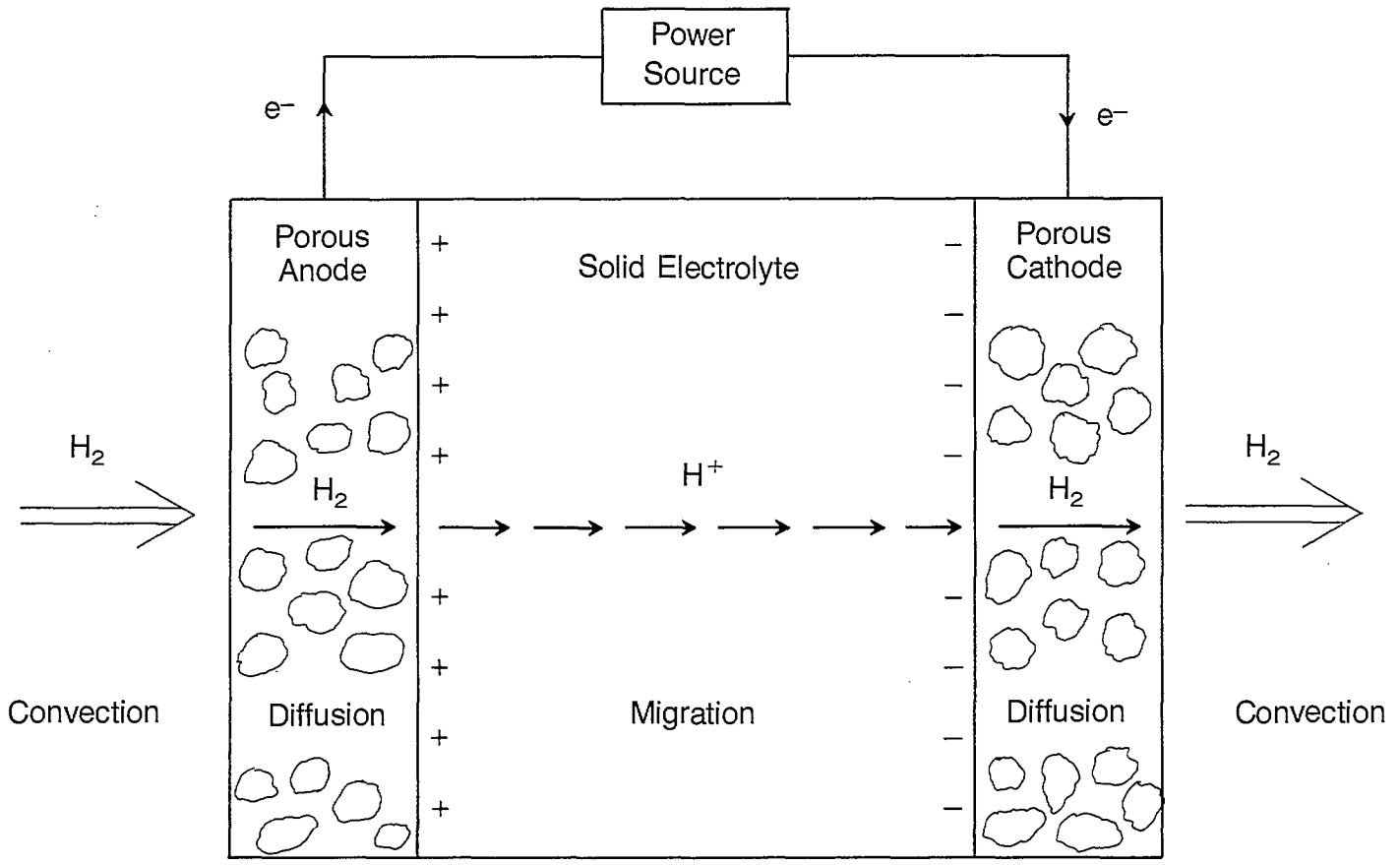

Fig. 4 - Mass transfer mechanisms for the three-phase, solid protonic-electrolyte system

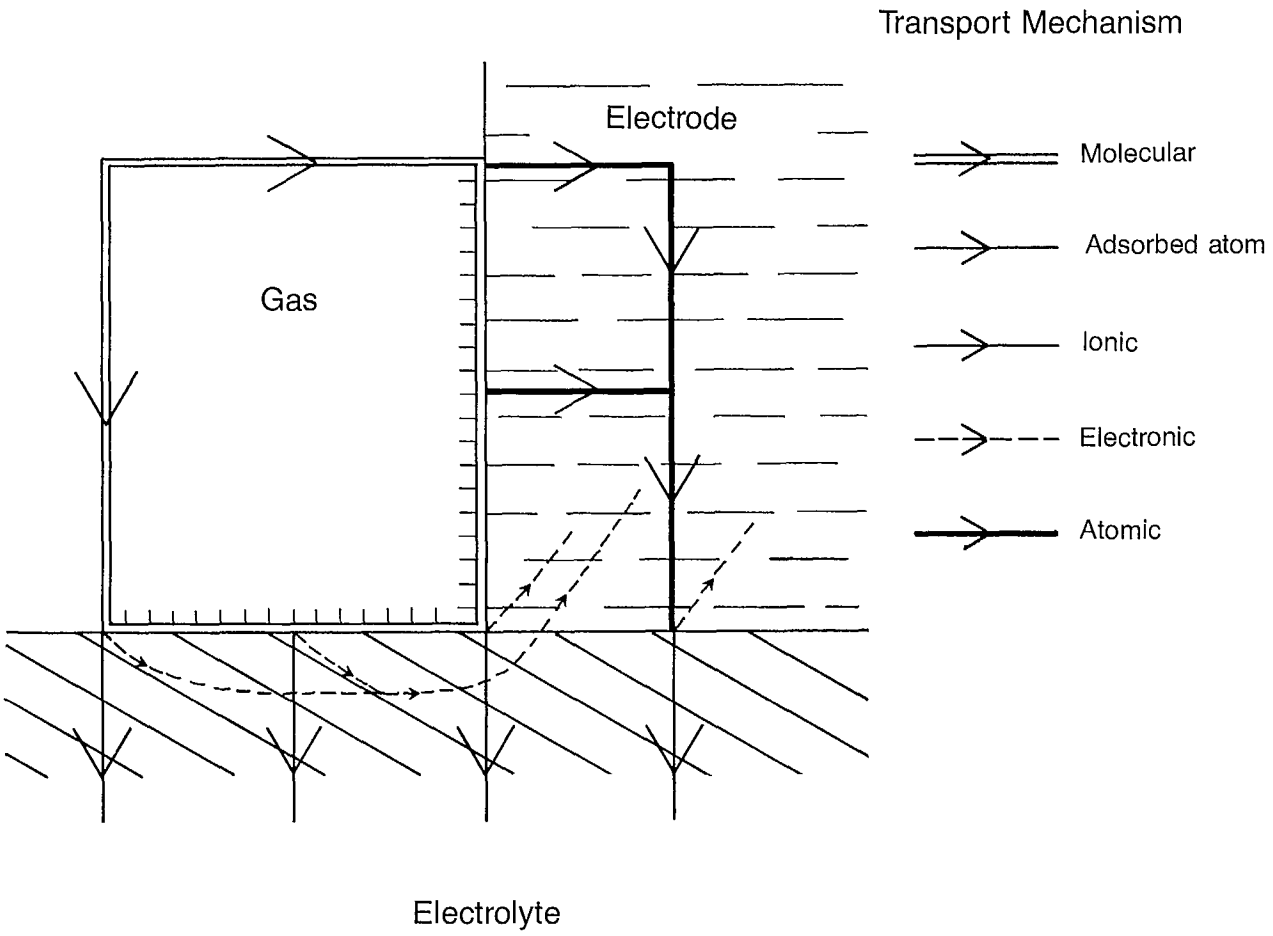

Fig. 5 - Material transport routes at the three-phase interface region (18)

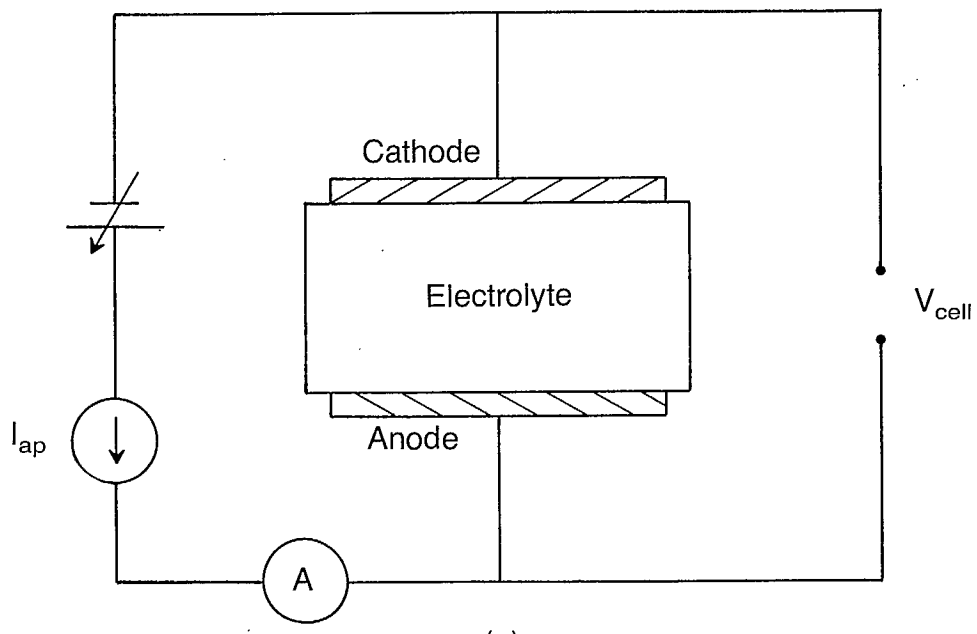

(a)
Two-probe cell

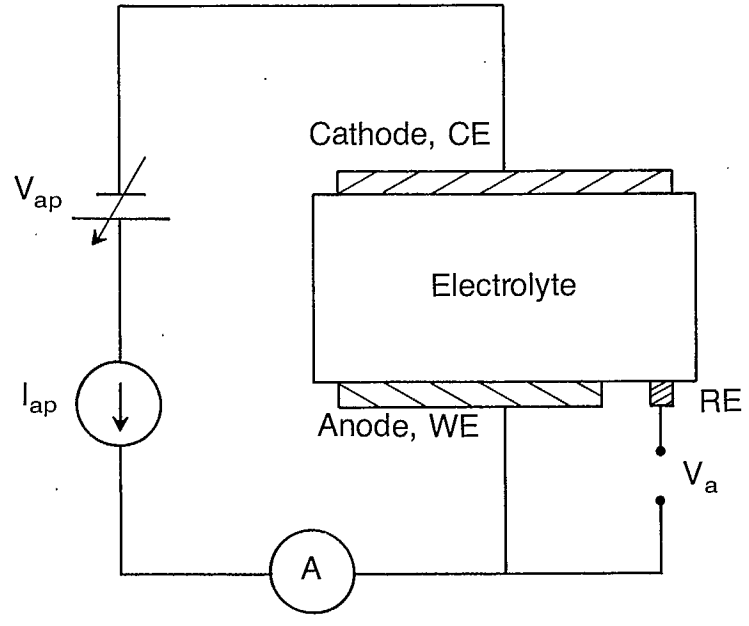

(b)
Three-probe cell

Fig. 6 - Two- and three-probe cells with solid electrolytes

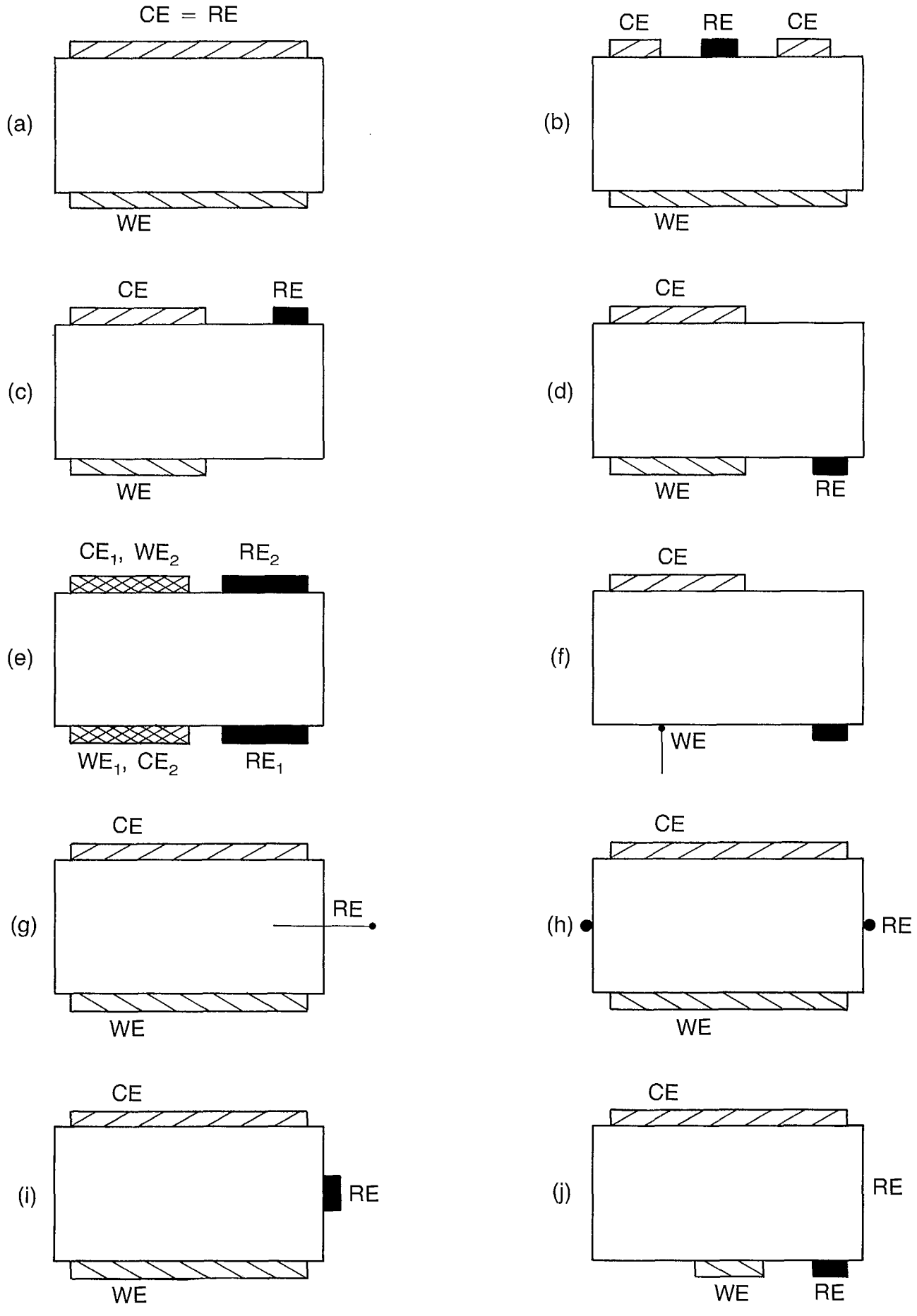

Fig. 7 - Three-phase solid electrolyte cell configurations

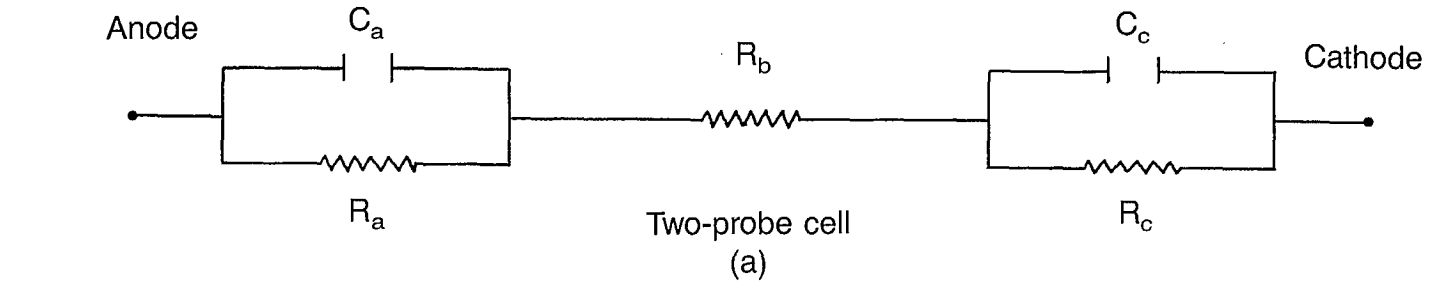

Two-probe cell
(a)

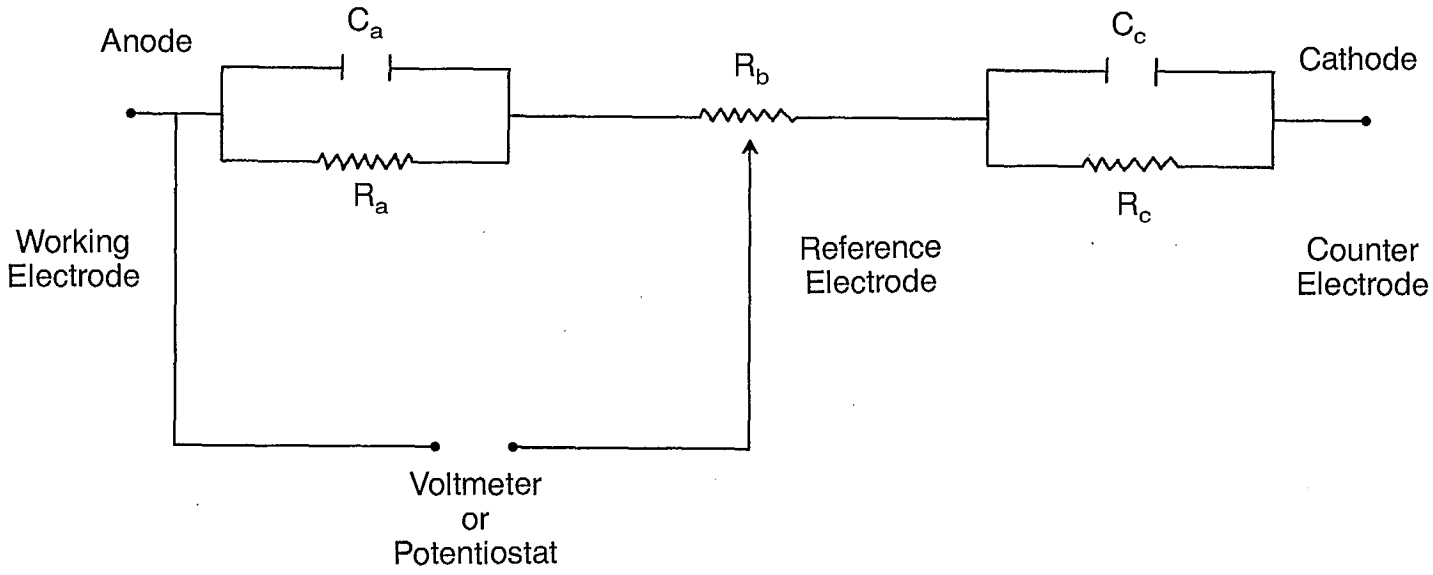

Three-probe cell
(b)

Fig. 8 - Equivalent circuits for two- and three-probe cells

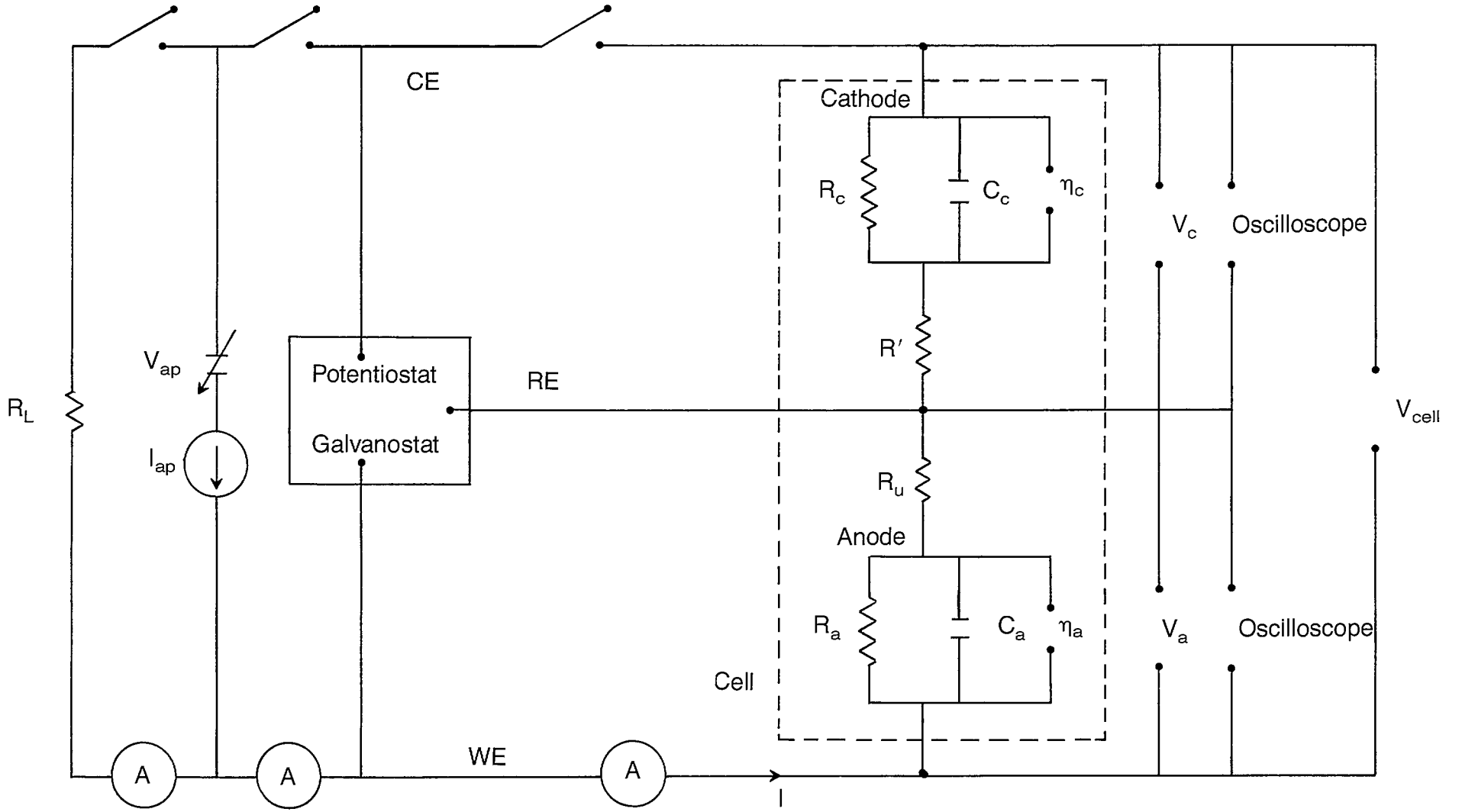

Fig. 9 - General experimental arrangement for two- and three-probe measurements

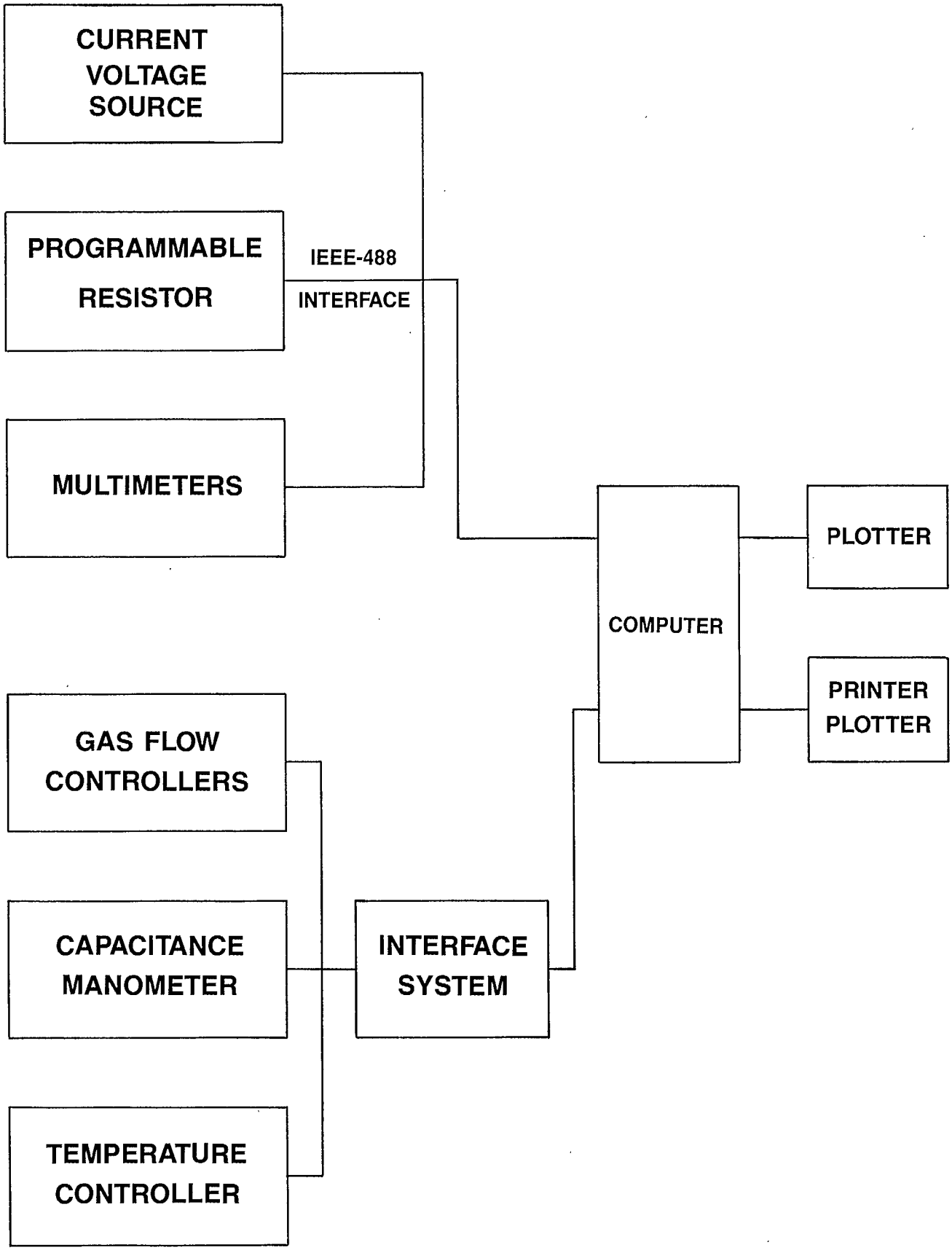

Fig. 10 - An automated system for electrochemical cell measurements

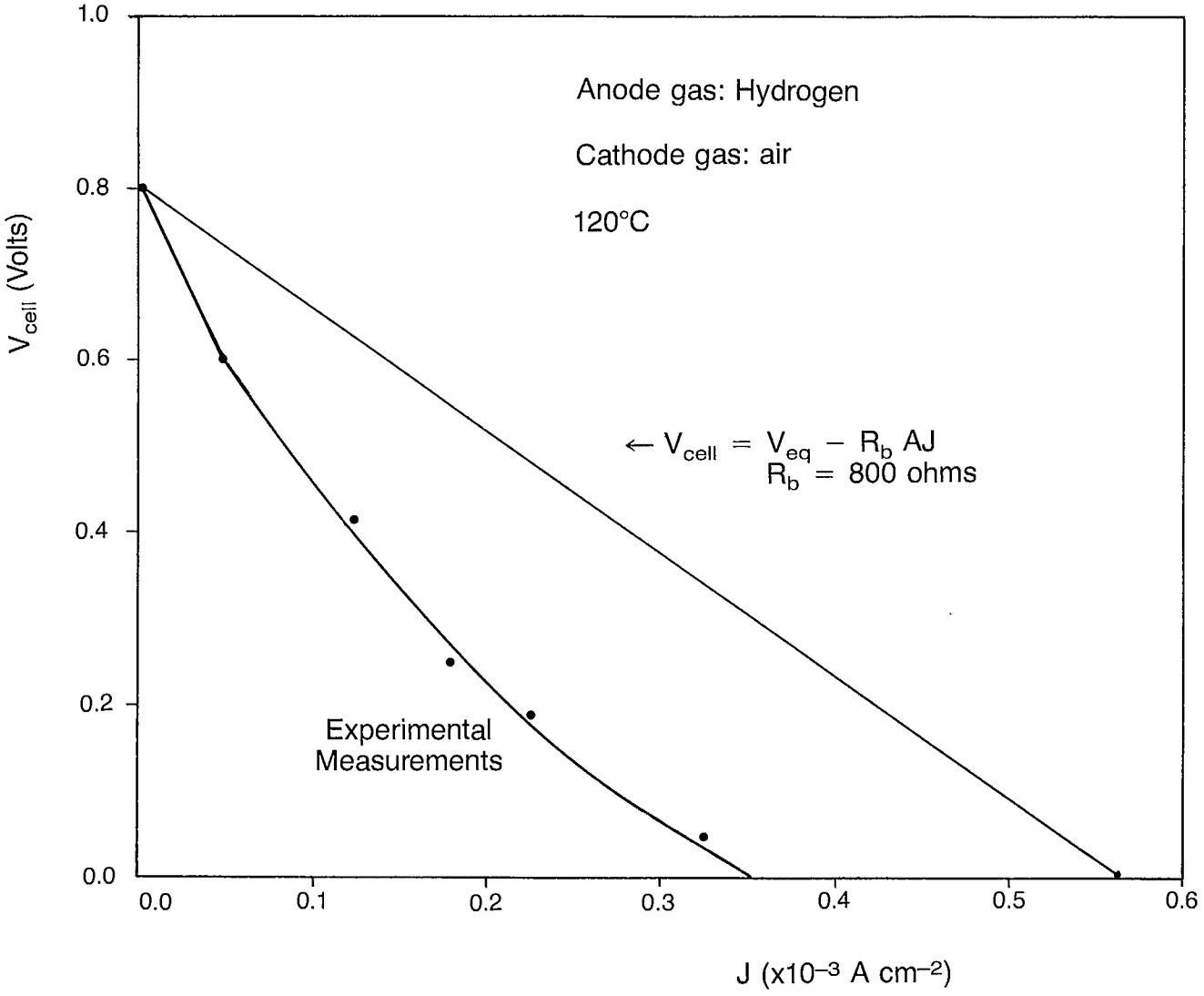

Fig. 11 - Fuel cell discharge experiment

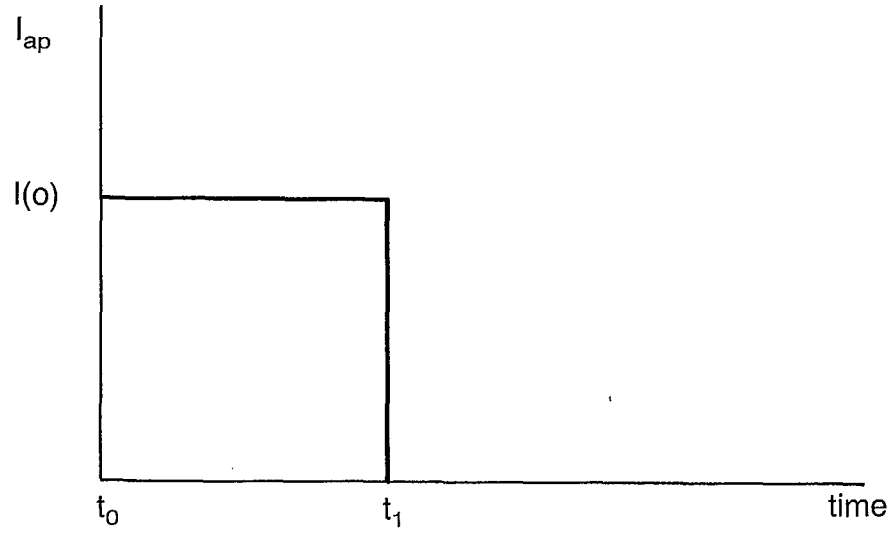

(a)
Current waveform

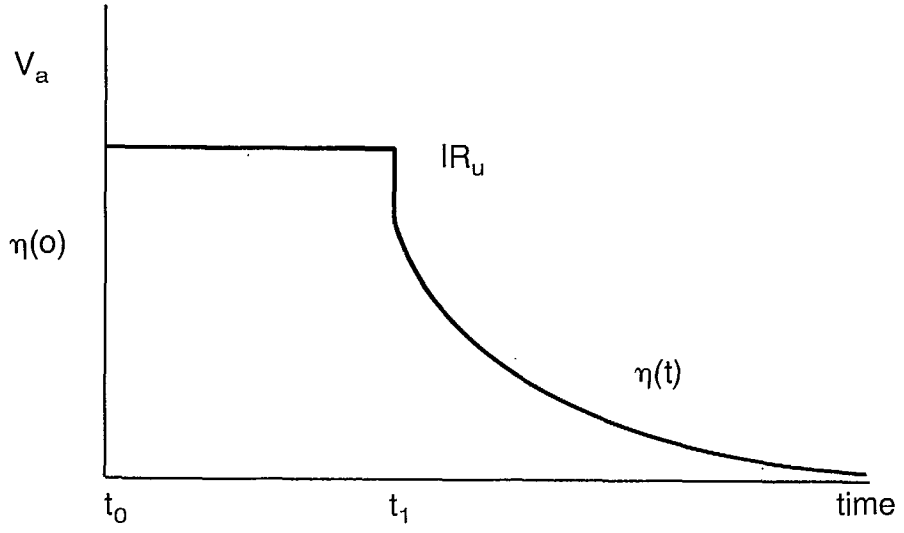

(b)
Anodic voltage waveform

Fig. 12 - Waveforms of the current-interruption method

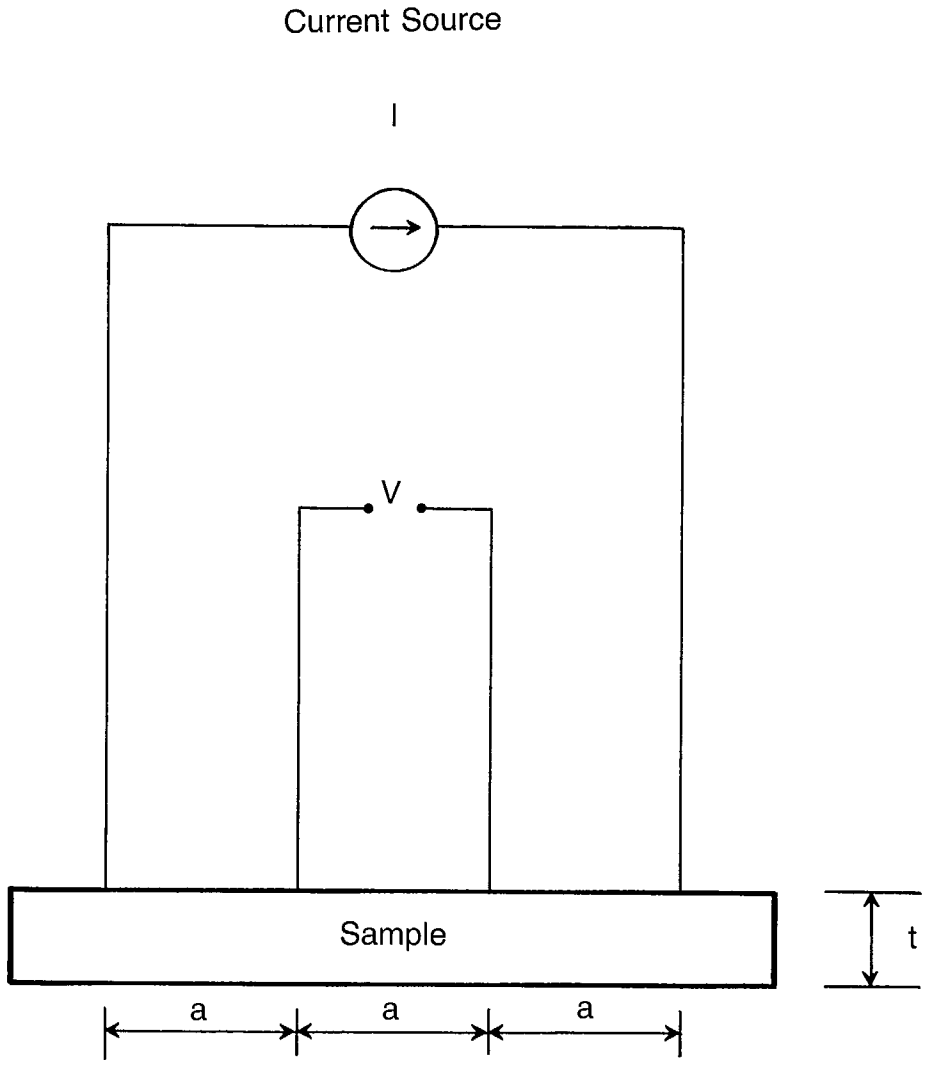

Fig. 13 - Schematic diagram of the four-probe measurement technique

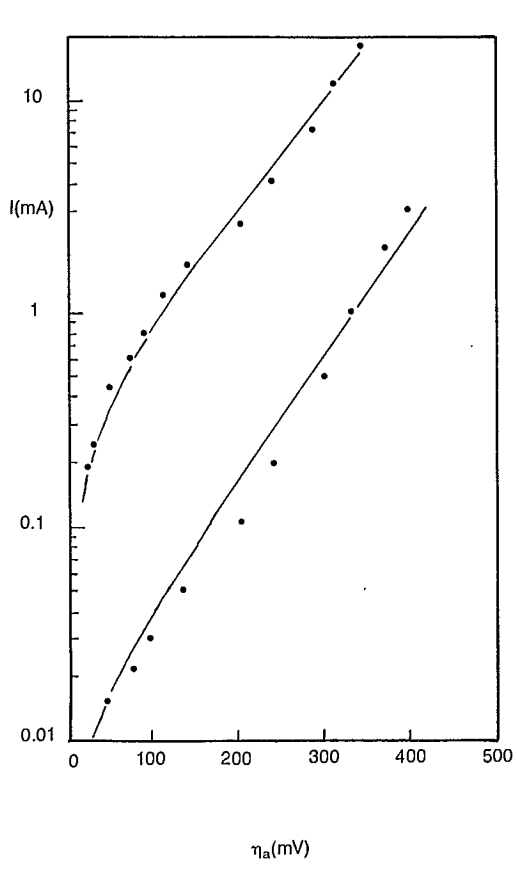

(a)
Anodic overpotential

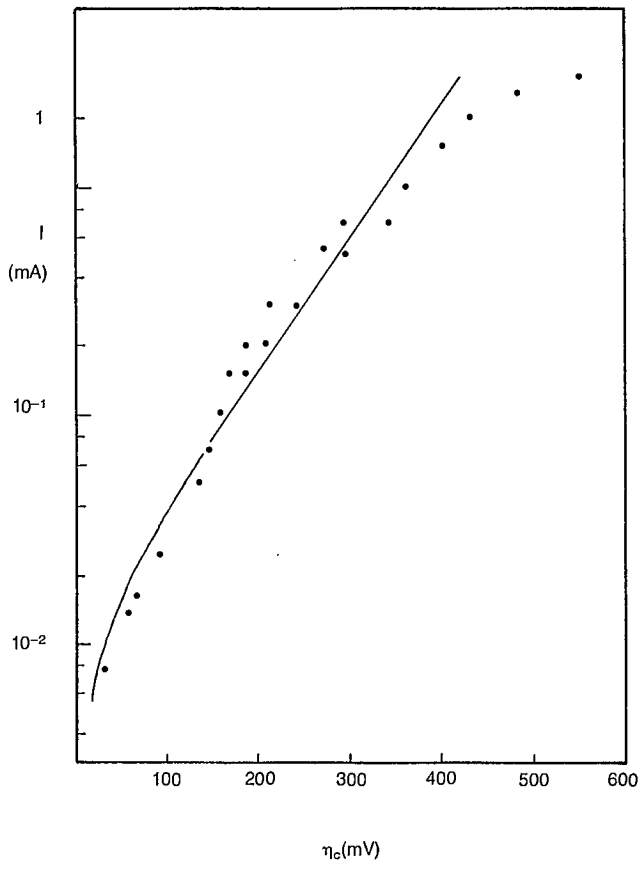

(b)
Cathodic overpotential

Fig. 14 - Overpotential curves obtained with the current-interrupt method

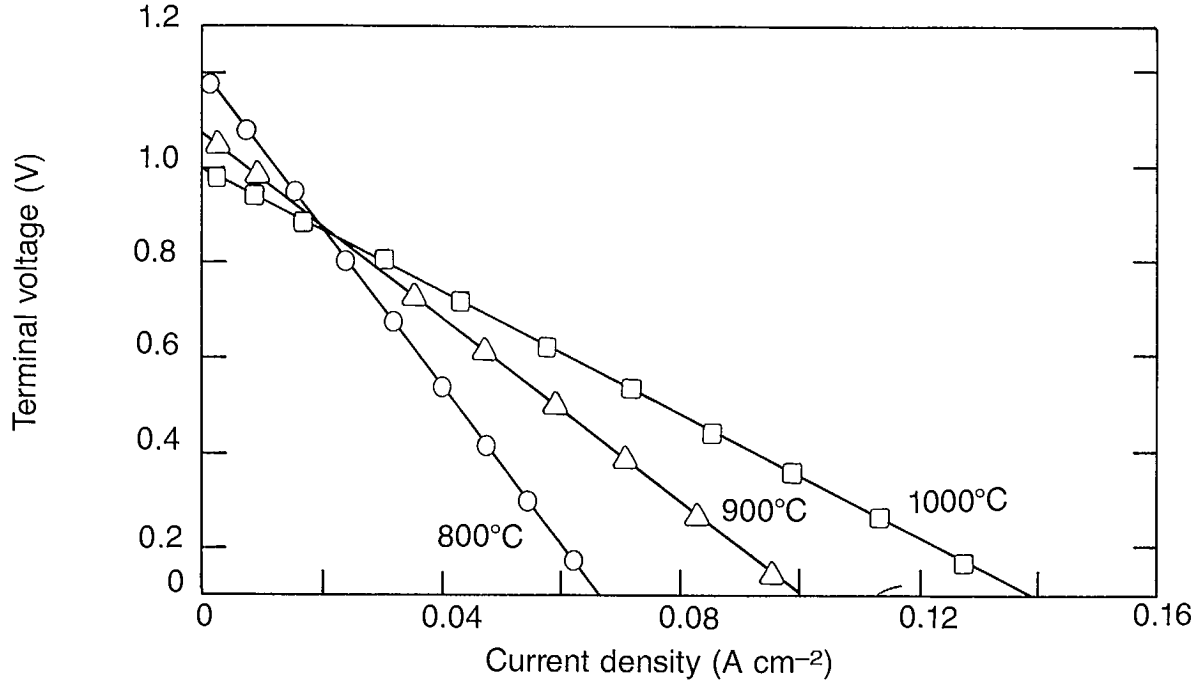

(a)
Performance of the cell

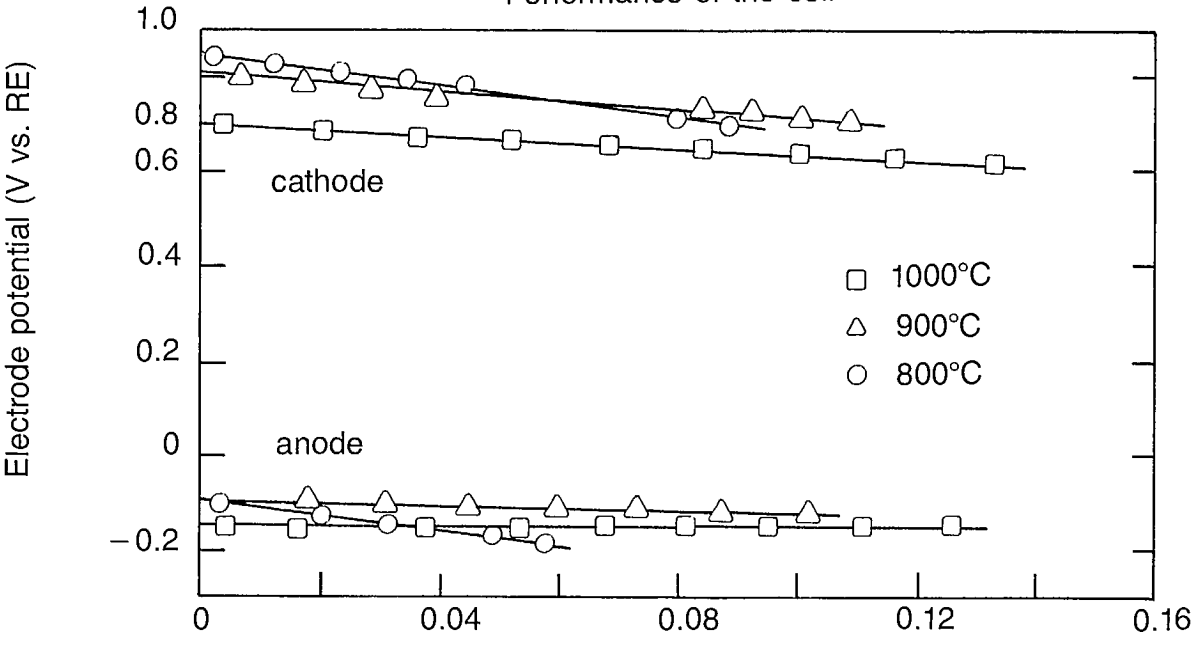

(b)
Polarization of the electrodes

Fig. 15 - Cell performance and electrode polarization for $SrCeO_3$